



## OPEN ACCESS

## EDITED BY

Rafael Almeida,  
San Diego State University, United States

## REVIEWED BY

Derman Dondurur,  
Dokuz Eylül University, Türkiye  
Wei Li,  
South China Sea Institute of Oceanology  
(CAS), China

## \*CORRESPONDENCE

Lyndon P. Nawanao Jr,  
✉ lpnawanao@up.edu.ph

## SPECIALTY SECTION

This article was submitted  
to Marine Geoscience,  
a section of the journal  
Frontiers in Earth Science

RECEIVED 27 September 2022

ACCEPTED 31 January 2023

PUBLISHED 03 March 2023

## CITATION

Nawanao LP Jr and Ramos NT (2023),  
Frontal wedge variations and controls of  
submarine landslides in the Negros–Sulu  
Trench System, Philippines.  
*Front. Earth Sci.* 11:1054825.  
doi: 10.3389/feart.2023.1054825

## COPYRIGHT

© 2023 Nawanao and Ramos. This is an  
open-access article distributed under the  
terms of the [Creative Commons  
Attribution License \(CC BY\)](https://creativecommons.org/licenses/by/4.0/). The use,  
distribution or reproduction in other  
forums is permitted, provided the original  
author(s) and the copyright owner(s) are  
credited and that the original publication  
in this journal is cited, in accordance with  
accepted academic practice. No use,  
distribution or reproduction is permitted  
which does not comply with these terms.

# Frontal wedge variations and controls of submarine landslides in the Negros–Sulu Trench System, Philippines

Lyndon P. Nawanao Jr\* and Noelynna T. Ramos

Geomorphology and Active Tectonics Research Laboratory, National Institute of Geological Sciences, University of the Philippines Diliman, Quezon City, Philippines

Frontal wedge characteristics provide clues to the efficiency of the overriding slab for large displacement during megathrust and upper-plate earthquakes, whereas submarine landslides along active margins may trigger or amplify tsunamis. The lack of clear precursors of submarine failures poses difficulty in monitoring and providing real-time alert warning systems. With that, delineating submarine features along active margins, their spatial distribution, and controls provide valuable information in identifying regions susceptible to large submarine landslides and tsunami hazard assessments. In this study, we performed terrain and morphometric analyses on 20 m resolution bathymetry data to map submarine landslides, submarine canyons, and lineaments in the forearc margin of the Negros–Sulu Trench System in the Philippines. Lineaments are distributed mainly along the frontal wedge, where previous seismic surveys revealed that the mapped ridges are morphotectonic expressions of thrust sediments. The morphological variations of the four frontal wedge segments were attributed to heterogeneous sediment influx, convergence rates, and subduction processes. More than 1,200 submarine landslides and their morphometric parameters were delineated, and exploratory spatial analyses indicate clustering and underlying controls. The tendencies of prolate submarine landslides (high L/W) to significantly cluster along submarine canyons while oblate morphologies (low L/W) along the frontal wedge reflect the different environments and geomorphological conditions to form these contrasting shapes. Ubiquitous small submarine landslides are mainly controlled by submarine canyon systems at relatively shallow depths of <2 km, where high sediment influx from inland sources preconditions instability. Large submarine landslides (>0.5 km<sup>3</sup>), on the other hand, are significantly most clustered where the Cagayan Ridge seamount collides and subsequently subducts beneath the northernmost frontal wedge. This suggests the dominant role of seamount subduction and related tectonic processes causing slope steepening to mainly induce large submarine landslides. This study unveiled how submarine landslides vary morphologically depending on their spatial, geomorphological, and tectonic controls in the active margin. This new information provides clues in identifying offshore areas susceptible to large submarine landslides that may induce damaging tsunamis in the Negros–Sulu Trench System as well as in other active margins of similar underlying controls.

## KEYWORDS

frontal wedge, submarine landslides, Negros–Sulu Trench System, Sulu Sea, submarine canyons, exploratory spatial analyses

## 1 Introduction

Submarine landslides occur when driving stresses on sediment layers increase or when shearing resistance decreases and are mainly triggered and preconditioned by the following: earthquakes, slope steepening, volcanic eruptions, rapid loading causing overpressure, wave and tidal loading, rapid sediment loading, gas hydrates, fluid migration, and weak stratigraphic layers (Vanneste et al., 2013; Scarselli 2020; Watson et al., 2020). Moreover, submarine landslides can induce tsunamis. This occurs when seafloor vertical displacement is translated into the seawater column and is a function of submarine landslide volume, depth, acceleration, velocity, and fluid density (Harbitz et al., 2014; Yavari-Ramshe and Ataie-Ashtiani 2016; Løvholt et al., 2017; Baba et al., 2019). Complex triggering factors with no clear precursors are the main challenges in creating an effective real-time early-warning system for submarine landslide-driven tsunamis.

In the past, submarine landslides were overlooked to cause damaging tsunamis until the 1998 Papua New Guinea submarine slump. This event caused a 15 m wave height leading to more than 2,200 fatalities that reshaped the perspective on the impacts of submarine landslides (Heinrich et al., 2001; Tappin 2021). Advancements in seafloor mapping and tsunami modeling have also led to revisiting past tsunamis that were once attributed only to earthquakes. Tsunami modeling of the following events was found to either be amplified or mainly induced by an earthquake-triggered submarine landslide: 1908 Mw 7.1 Messina (12 m maximum tsunami, 80,000 fatalities) (Schambach et al., 2020), 1945 Mw 8.1 Makran (15 m, 4,000) (Rastgoftar and Soltanpour 2016), 1946 Ms 7.1 Aleutian (16 m, 167) (Fryer et al., 2004), 1964 Mw 9.2 Alaska (12 m, 131) (Parsons et al., 2014), 1992 Ms 7.5 Flores Island (26 m, 1,713) (Hidayat et al., 1995; Imamura et al., 1995), 1994 Mw 7.1 Mindoro (7 m, 78) (Ramirez et al., 2022), as well as the more recent 2011 Mw 9.0 Tohoku (40 m, 18,490) (Tappin et al., 2014) and 2018 Mw 7.5 Sulawesi (10 m, 2,000) (Takagi et al., 2019; Nakata et al., 2020) tsunami events.

The 1945 Makran, 1946 Aleutian, 1964 Alaska, 1992 Flores Island, and 2011 Tohoku tsunami events occurred along active margins, where subduction processes predominantly trigger submarine failures. Recent studies linked the distribution of submarine landslides in forearc basins to seismic loading, oversteepening of the frontal wedge, seamount subduction, and submarine canyon development (Mountjoy et al., 2009; Pedley et al., 2010; Watson et al., 2020). The frontal wedge is of particular interest as its configuration implicates the variability of subduction processes along the trench. This includes whether a trench segment undergoes accretion or erosion (e.g., Kao et al., 2000; Pedley et al., 2010; Armada et al., 2020) as well as the relationship between the frontal wedge morphometry and maximum tsunami wave heights for megathrust earthquakes (Qiu and Barbot 2022). The link between the frontal wedge and subsequent submarine landslides was also documented in other active margins including the Nankai Trough (Moore et al., 2019), Hikurangi Trough (Pedley et al., 2010), and Java Trench (Kopp et al., 2006). These studies highlight the role of variability in subduction processes along the trench and the consequent submarine slope failures.

Mapping both the frontal wedge and other submarine features as well as conducting exploratory spatial statistics can be significant

initial steps toward providing informed decisions in minimizing the impacts and inferring seafloor areas that are susceptible to tsunamigenic submarine landslides (e.g., Völker, 2010; Kawamura et al., 2012; Parsons et al., 2014; Watson et al., 2020; Gamboa et al., 2022).

The Philippines is an archipelago surrounded by subduction zones with the potential to generate strong to great earthquakes that can trigger submarine landslides. Despite its active seismicity and tectonics, the Negros–Sulu Trench System (NSTS) remains understudied, and its submarine geomorphological features are poorly constrained. In this study, we mapped the frontal wedge variations, submarine canyons, lineaments, and submarine landslides in the active margin of the Sulu Sea using high-resolution multibeam bathymetry data. Furthermore, this study aims to infer the controls of submarine landslides through their morphometric parameters and exploratory spatial analyses. For the first time, the morphological characteristics of these submarine features in the NSTS are examined in detail, with a particular focus on the morphological variations and spatial distribution of submarine landslides.

## 2 Sulu Sea tectonic setting and historical tsunamis

The NSTS is an active margin where the Sulu Sea subducts beneath the Philippine Mobile Belt (PMB). This marginal basin is enclosed by the Zamboanga Peninsula and the islands of Sulu, Panay, Negros, and Palawan. The Sulu Sea is divided into four major tectonic terranes: northwest Sulu basin (NWS), Cagayan Ridge (CR), southeast Sulu basin (SES), and the accretionary prism (AP) along the NSTS (Rangin, 1989). The Palawan Microcontinental Block (PCB) terrane occupies north of the Sulu Sea. The NWS has thicker crust (>10 km) than the SES (6 km), and between these two sediment-filled sub-basins is the Cagayan Ridge seamount composed of basalt, tuff, and andesite (Rangin and Silver 1990) (Figure 1). GPS surveys revealed that this trench system generally has low convergence rates (<60 mm yr<sup>-1</sup>) (Rangin et al., 1999; Simons et al., 1999). Two prominent models suggest that the Sulu Sea was formed due to back-arc rifting from the subduction of either the proto-South China Sea along the Cagayan Arc (e.g., Bellon & Rangin, 1991; Rangin & Silver, 1991; Schlüter et al., 2001; Liu et al., 2014) or the Celebes Sea along the Sulu and Zamboanga Peninsula Arc (Rangin, 1989; Hall 2002, 2013, 2012; Lai et al., 2021).

Since 1589, three historical tsunamigenic earthquakes occurred along the NSTS: 1897 Ms 7.5, 1925 Ms 6.8, and 1948 Ms 8.2 events (Bautista et al., 2012). The 1897 earthquake event had an epicenter near the Zamboanga Peninsula and generated up to a 6 m tsunami that widely affected the coastal areas in the Sulu Sea. The basin-wide distribution and maximum tsunami wave height for a Ms 7.5 earthquake pose questions regarding its mechanism. Whether this event was a tsunami earthquake or triggered by a submarine landslide is still unknown. On the other hand, the 1925 and 1948 earthquake events generated a tsunami of up to 2 m that only affected southeastern Negros and Panay islands, respectively. The 1948 event is distinct among the three as its epicenter is inland. The rupture parameters of these tsunamigenic earthquakes, however, are still poorly constrained.

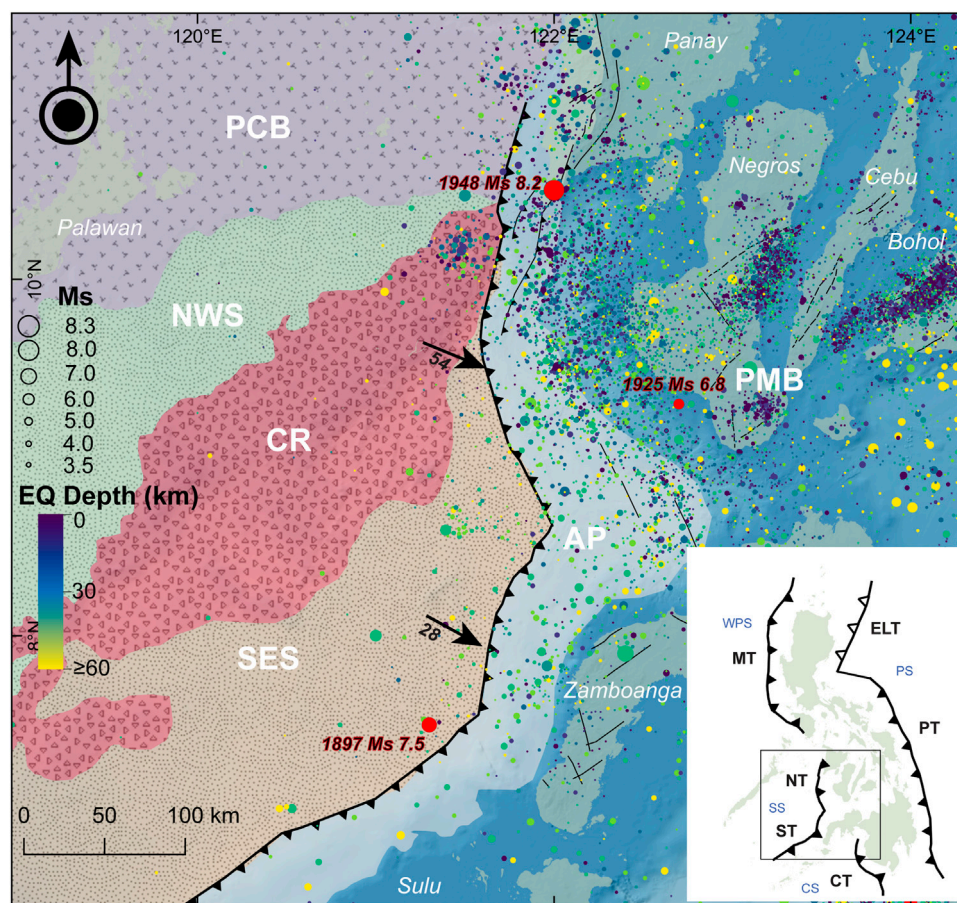


**FIGURE 1**

The Sulu Sea Basin and nearby tectonic features. Major tectonic terranes in the Sulu Sea include the northwest Sulu basin (NWS), Cagayan Ridge (CR), southeast Sulu basin (SES), and accretionary prism (AP) along the Negros–Sulu Trench System (NSTS). The Palawan Microcontinental Block (PCB) consists of continent-derived lithologies rifted from the eastern Eurasian margin, while the arc-derived Philippine Mobile Belt (PMB) comprises the rest of the archipelago (modified from Rangin, 1989). Arrows indicate the velocity vectors ( $\text{mm yr}^{-1}$ ) from continuous GPS campaigns (1994–1996) across the Philippines (Rangin et al., 1999; Simons et al., 1999). Red circles indicate the epicenter of the three historical tsunamigenic earthquakes in the Sulu Sea (Bautista et al., 2012). The onshore faults, lineaments (black lines), and catalog (1589–2020) of surface-wave magnitude (Ms) earthquakes (EQ) are from PHIVOLCS. The inset map shows the location of the Sulu Sea (SS) and the other surrounding basins (West Philippine Sea, WPS; Cotabato Sea, CS; Philippine Sea, PS) and trenches (Manila Trench, MT; Negros Trench, NT; Sulu Trench, ST; Cotabato Trench, CT; Philippine Trench, PT; East Luzon Trough, ELT).

### 3 Materials and methods

#### 3.1 Delineating submarine landslides and their morphological parameters, submarine canyons, and lineaments

The bathymetry data of the National Mapping and Resource Information Authority (NAMRIA) has a 20 m resolution and a depth accuracy of 1 m. These were collated from the multibeam bathymetric surveys in the Sulu Sea between 1999 and 2018 by the NAMRIA and the Naval Oceanographic Office (NAVOCEANO, United States). Terrain analyses were applied to the bathymetry data including slope, roughness, and hillshade. Slope was derived using the algorithm of Horn (1981). By showing both the slope and depth through transparency adjustments, submarine landslides, canyons, and lineaments were mapped. To delineate submarine

canyons, drainage extraction algorithms in ArcGIS were utilized including *flow direction* and *flow accumulation*.

The submarine landslides were mapped based on the following key morphological features: head scarp (scar) characterized by a relatively steep slope at the top of the landslide, arcuate or concave morphology of the landslide area, and the presence of mass transport deposits (MTDs) at the toe of the landslide (Watson et al., 2020). Majority of the mapped landslides, however, are based mainly on head scarp and arcuate morphologies due to the rare occurrence of MTDs observed. The apparent rare occurrence of MTDs is attributed to the resolution of the bathymetry and the low preservation of these deposits once disintegrated. Interactive 2D cross-sectional profiles in QGIS also aided in recognizing the concave morphology of submarine landslides, especially at smaller scales. The submarine landslides are further categorized into four levels (1–4) of confidence scale (Watson et al., 2020) based on the presence of key morphological features of submarine landslides (Figure 2).

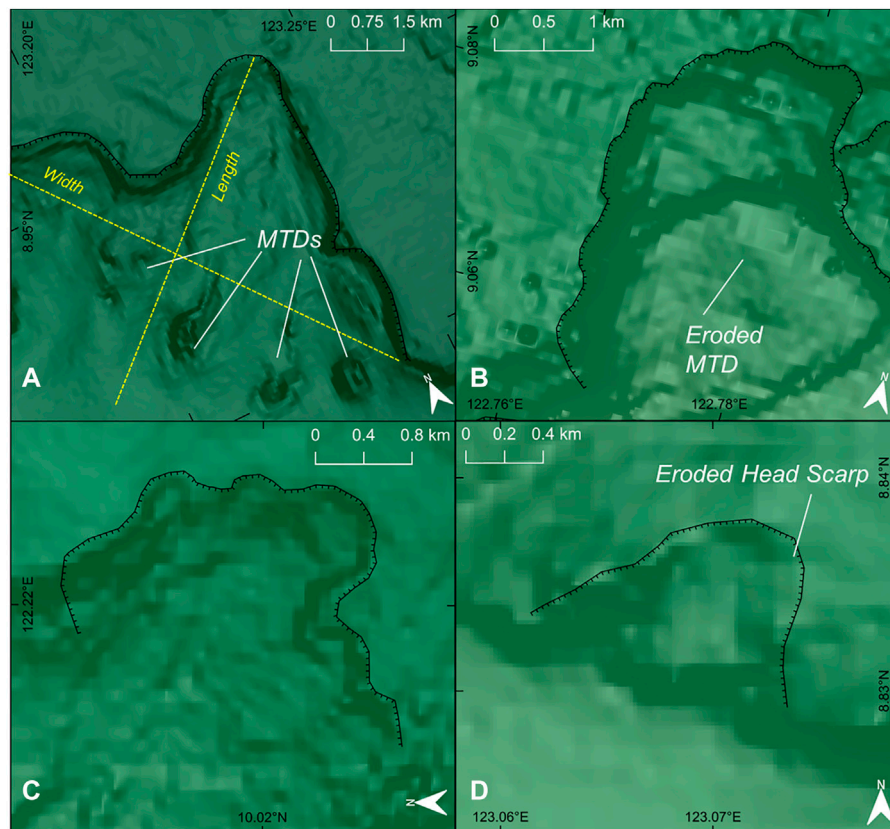


**FIGURE 2**

Landslide morphometric parameters (length, width, MTDs, head scarp) and confidence classification based on Watson et al. (2020). (A) Category 1: well-defined head scarp, arcuate morphology, and MTD at the toe. (B) Category 2: well-defined head scarp and arcuate morphology, eroded to no clear indication of MTDs. (C) Category 3: presence of head scarps, although eroded, and arcuate morphology. No MTDs. (D) Category 4: Heavily eroded headscarps and no MTDs but with arcuate morphology; these are mainly small submarine landslides limited by the bathymetry resolution.

Table 1 shows the delineated morphometric parameters of submarine landslides modified after Gamboa et al. (2022) and Watson et al. (2020). Volume, in particular, was estimated by first creating a pre-landslide digital elevation model (DEM) similar to the methods of Gamboa et al. (2022). The pre-landslide DEM is estimated by sampling elevations around the perimeter of the landslide and applying a multi-level b-spline interpolation at a larger 100 x 100 m raster grid. Volume is calculated based on the surface difference between the pre-landslide DEM as the top surface and the present bathymetry data as the base. Figure 3 shows a sample of the modeled pre-landslide surface and the present scarp morphology for volume calculation.

### 3.2 Statistical analyses of submarine features

Two-dimensional (2D) histograms were applied among the morphometric parameters to infer correlations. Ripley's L function (Ripley 1977) was calculated through the *spatstat* package in R to determine whether the distribution of submarine landslides has significant clustering across different distance scales.

The L function is a linear transformation of the K function expressed in distance and calculated by:

$$L(r) = \sqrt{\frac{K(r)}{\pi}} = \sqrt{\frac{A \sum_{i=1}^n \sum_{j=1, j \neq i}^n k(i, j)}{\pi n(n-1)}} \quad (1)$$

where  $A$  = area of the bathymetry coverage,  $n$  = total number of mapped submarine landslides,  $r$  = distance, and  $k(i, j)$  is the weighting factor for edge detection. A neighboring ( $j$ ) submarine landslide is included in the summation when its distance from the reference submarine landslide ( $i$ ) is  $\leq r$ . The centroid of each submarine landslide served as an input point. Observed  $L(r)$  greater than the expected values indicate significant clustering, whereas lower observed  $L(r)$  suggest dispersion. A total of 999 permutations were run to calculate the confidence interval (CI) envelope of the  $L(r)$  signifying complete spatial randomness.

Kernel density analysis was performed in ArcGIS to estimate the 2D probability density distribution (Silverman 1986) of the delineated submarine landslides, submarine canyons, and lineaments. The distribution of earthquakes (1589–2020) from the Philippine Institute of Volcanology and Seismology (PHIVOLCS) was also included in the kernel estimation. Kernel

**TABLE 1** Delineated morphometric parameters of submarine landslides modified from Gamboa et al. (2022) and Watson et al. (2020).

Parameter	Description
Minimum depth (top depth)	Submarine landslide depth (km) of the head scarp
Maximum depth	Submarine landslide depth (km) of the toe
Mean depth	Mean depth (km) within the landslide area
Height	Difference between the maximum and minimum depths (km)
Head scarp length	Length (km) of the landslide head scarp
Area	Area of the landslide polygon (km <sup>2</sup> )
Length	Landslide length perpendicular to the contour and flow direction (km)
Width	Landslide width, i.e., the widest distance within the landslide area perpendicular to the length (km)
L/W	Length-to-width ratio
Maximum slope	Highest slope within the submarine landslide area, typically along the head scarp (°)
Mean slope	Mean slope within the submarine landslide area (°)
Volume	Estimated volume (km <sup>3</sup> ) of the submarine landslide based on the difference between the surface of the modeled pre-landslide and present landslide DEM
Distance from trench	The shortest distance of the submarine landslide from the trench (km)
Distance from submarine canyon	The shortest distance of the submarine landslide from a submarine canyon (km)

density can provide insights into the intensity variation, spatial correlation among submarine features, and underlying processes that may be linked to the distribution of submarine landslides. These kernel densities are further evaluated through correlation matrices of the raster bands between submarine landslides and submarine canyons, lineaments, and earthquakes.

To examine statistically significant clusters of relatively large- and small-volume submarine landslides, we identified their spatial distribution using the Getis-Ord ( $G_i^*$ ) statistic (Getis and Ord 1992) that calculates the z-score and equivalent  $p$ -values of each submarine landslide:

$$G_i^*(d) = \frac{\sum_{j=1}^n w_{i,j} x_j - \bar{x} \sum_{j=1}^n w_{i,j}}{s \sqrt{\frac{n \sum_{j=1}^n w_{i,j}^2 - (\sum_{j=1}^n w_{i,j})^2}{n-1}}} \quad (2)$$

where  $G_i^*$  = z-score,  $x_j$  = volume,  $w_{i,j}$  = weighting factor based on the spatial relationship of  $i$  and  $j$  neighbors at distance  $d$ ,  $\bar{x}$  = mean sample volume, and  $s$  = volume standard deviation among neighbors. The *optimized hot spot analysis* in ArcGIS based on Getis-Ord assigns a fixed distance  $d$  based on the first peak clustering (=14.3 km). Submarine landslides were then grouped into seven: one that belongs to null groups (1), three that belong to significant clusters of high values at 99% confidence interval (CI) (2), 95% CI (3), 90% CI (4), and three that belong to significant clusters of low values at 99% CI (5), 95% CI (6), and 90% CI (7). These groups are then compared based on select morphometric parameters using boxplots. In addition to volume, another morphometric parameter that was calculated with  $G_i^*$  is the length-to-width ratio (L/W) to explore significant clusters of prolate (high L/W) and oblate (low L/W) submarine landslides relative to the flow direction. Altogether, these exploratory spatial analyses aim to

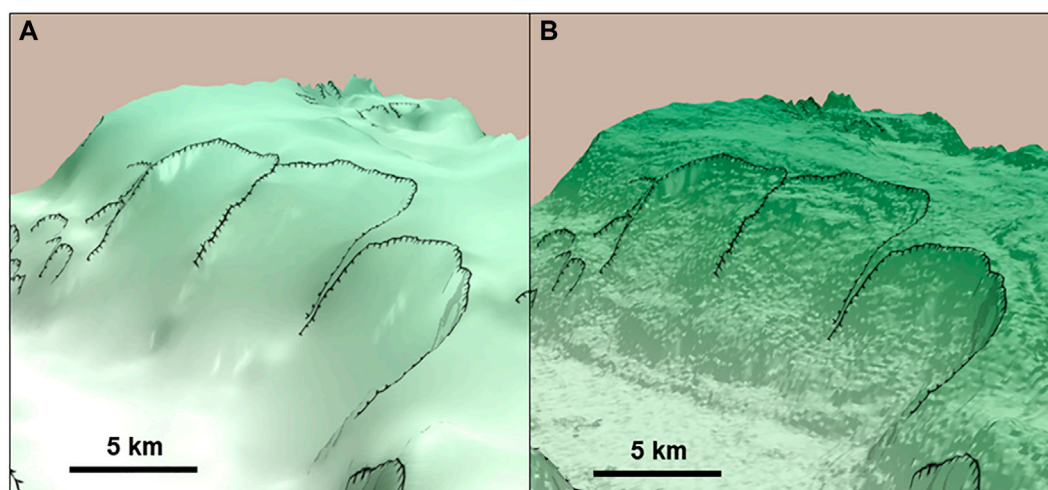


**FIGURE 3**

Three-dimensional (3D) perspective of the modeled pre-landslide and the present surface of the submarine landslides. (A) The modeled pre-landslide is calculated based on the multi-level b-spline calculation at a coarser 100 x 100 m resolution around the perimeter of the submarine landslide that represents the intact slope. (B) The present surface DEM serves as the base, whereas the modeled pre-landslide is the top surface for estimating the slump volume.

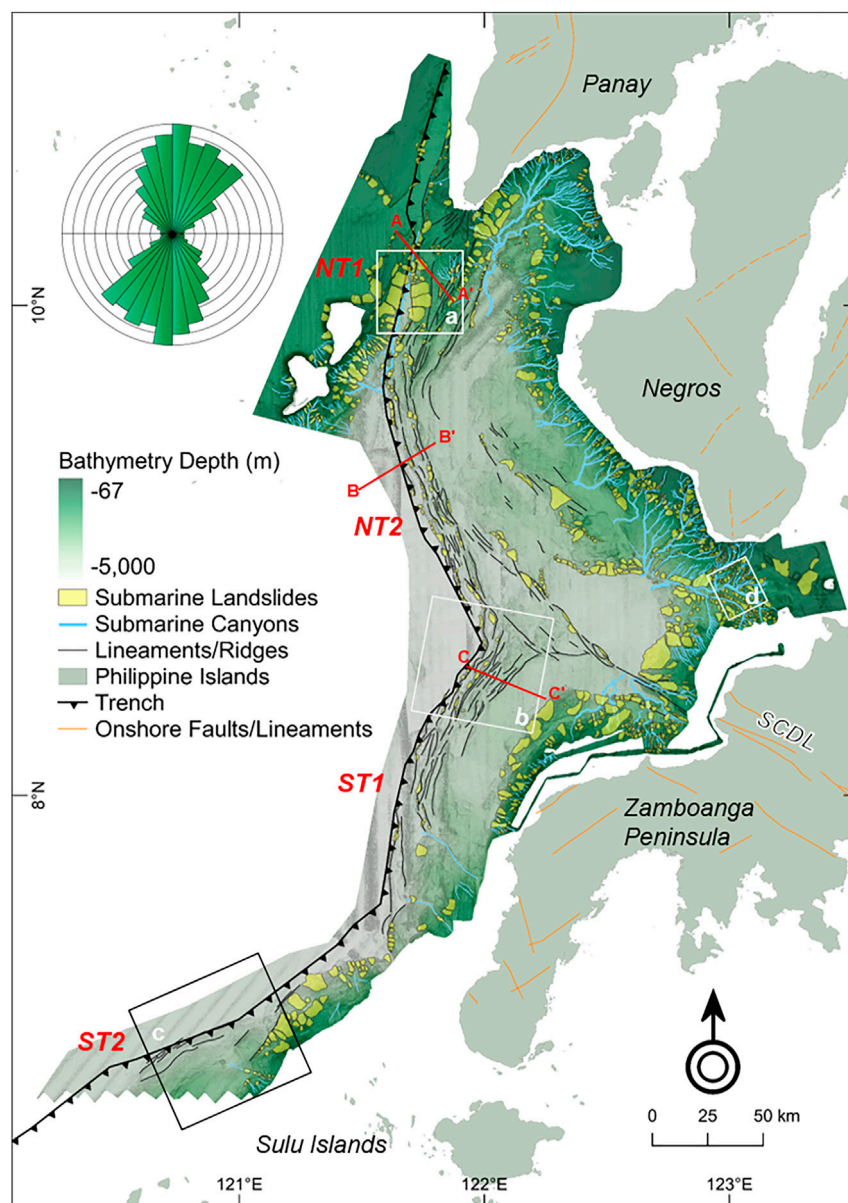


**FIGURE 4**

Submarine landslides, submarine canyons, and lineaments mapped in the active margin of the NSTS. Rose diagram shows the general northerly trend of the lineaments. Four segments (NT1, NT2, ST1, ST2) were delineated based on the orientation and width variations of the frontal wedge. Squares a–d show the locations of representative submarine features in Figure 5. Red lines are transects of seismic reflection profiles from Schlüter et al. (1996) (Figure 6). The northwest-trending lineaments mapped offshore of Zamboanga Peninsula are inferred to be an extension of the Sindangan–Cotabato–Daguma Lineament (SCDL) in western Mindanao Island (orange lines = onshore faults/lineaments from PHIVOLCS).

unravel spatial patterns, providing insights into the occurrence and controls of submarine landslides in the NSTS.

## 4 Results

### 4.1 Submarine landslides, submarine canyons, lineaments, and frontal wedge variations

A total of 1,214 submarine landslides were mapped (Figure 4) with 64.7% under category 4, 31.6% category 3,

3.1% category 2, and 0.6% category 1. The multitude of categories 3 and 4 reflects the limitation of the bathymetry resolution in readily discerning head scarp and arcuate morphologies but without traces of MTDs. Large networks of submarine canyons were mapped between Negros Island and Zamboanga Peninsula and between Panay and Negros islands. Submarine gullies develop at the shelf edge of about 180 m below sea level and interconnect with larger submarine canyons at deeper portions as slope abruptly increases (Figures 5D, E). Lineaments are mainly situated along the frontal wedge, occurring as parallel ridges, with the majority following a north-to-northeast trend. In addition, the northwest-trending

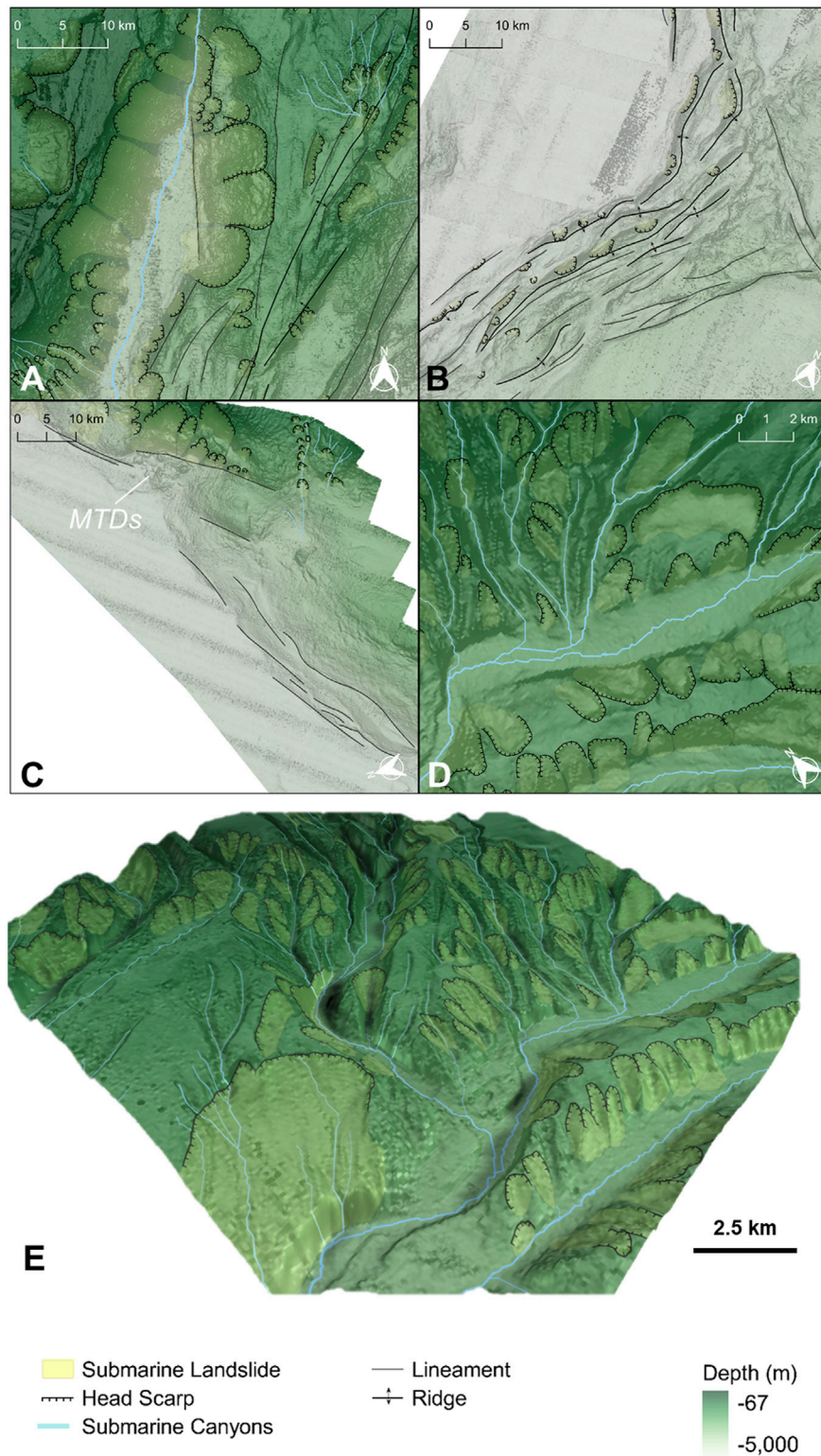


**FIGURE 5**

Close-up view of the mapped submarine features (see Figure 4 for their location). **(A)** Large submarine landslides along the steep frontal wedge of the northern NT segment (NT1) and steep bathymetry of the colliding Cagayan Ridge (CR) in the west. Between the frontal wedge and the CR is a deeply incised submarine canyon that is parallel to the trench. **(B)** Prominent deformation front and associated submarine features of the frontal wedge in the northern ST segment (ST1). **(C)** Poorly developed frontal wedge, submarine canyons, and submarine landslides in the southern ST segment (ST2). **(D)** Well-developed networks of submarine canyons and associated submarine landslides offshore of southern Negros island. **(E)** Three-dimensional perspective of submarine landslides in Figure 5D.

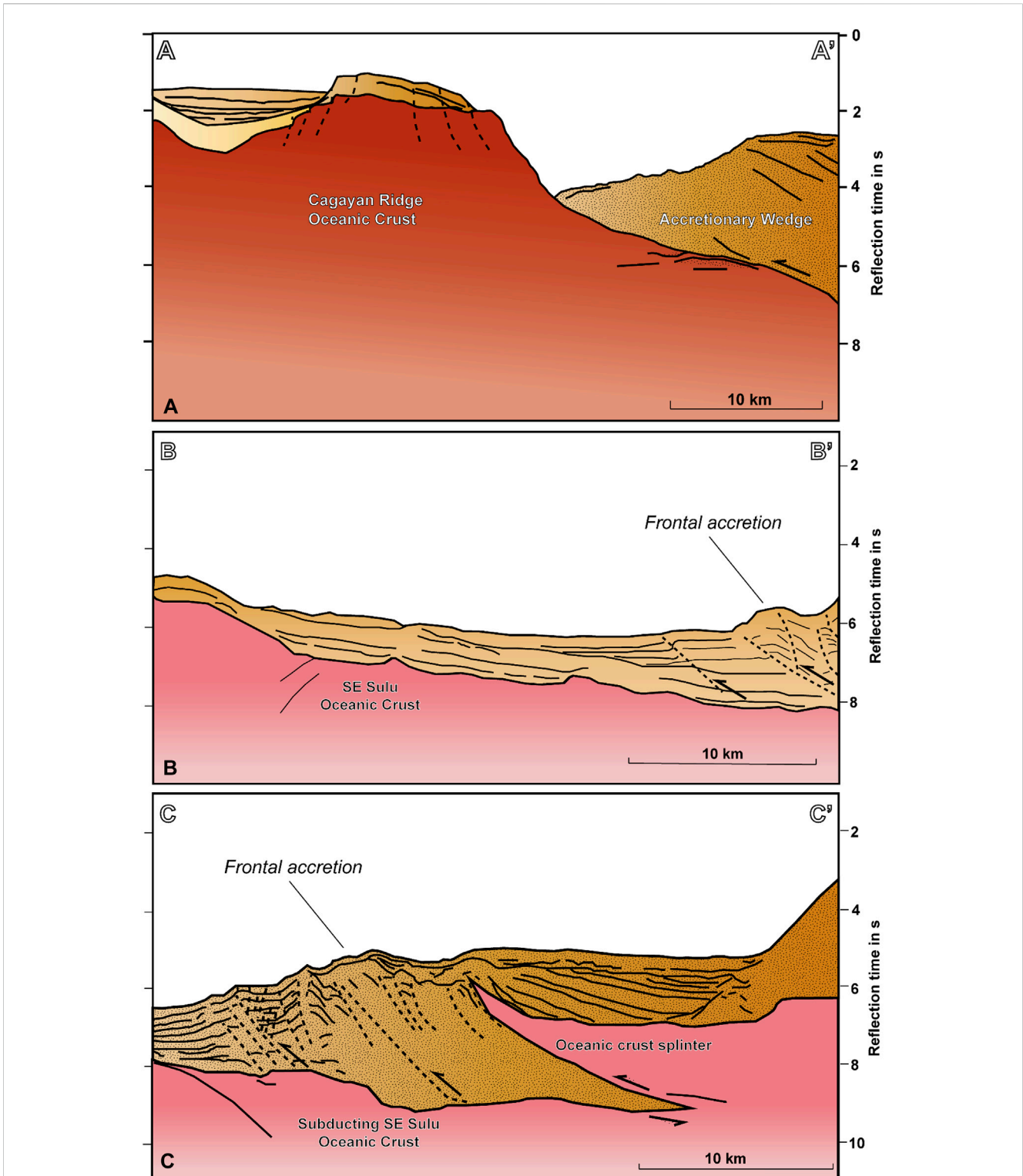


**FIGURE 6** Interpreted seismic reflection profiles (as shown in Figure 4) perpendicular to the frontal wedge (adapted from Schlüter et al., 1996 with permission from Elsevier). **(A)** (Line SO 49-16) Collision and subduction of the Cagayan Ridge seamount beneath the northern accretionary prism. **(B)** (Line SO 49-09) Reverse faults associated with the frontal accretion of sediments in the southern Negros Trench segment (NT2). **(C)** (Line SO 49-06) Dense high-angle reverse faults associated with frontal accretion in the northern Sulu Trench segment (ST1), manifested by dense lineaments and ridges as shown in Figure 5B. The identified oceanic splinter is linked to intense thrusting and folding along this segment.

lineaments offshore of Zamboanga Peninsula are inferred to be an extension of the Sindangan–Cotabato–Daguma Lineament (SCDL) (Pubellier et al., 1996) (Figure 4).

Interpreted seismic reflection profiles (Figure 6) by Schlüter et al. (1996) across the trenches revealed that these mapped frontal ridges are seafloor manifestations of accreted trench sediments thrust by

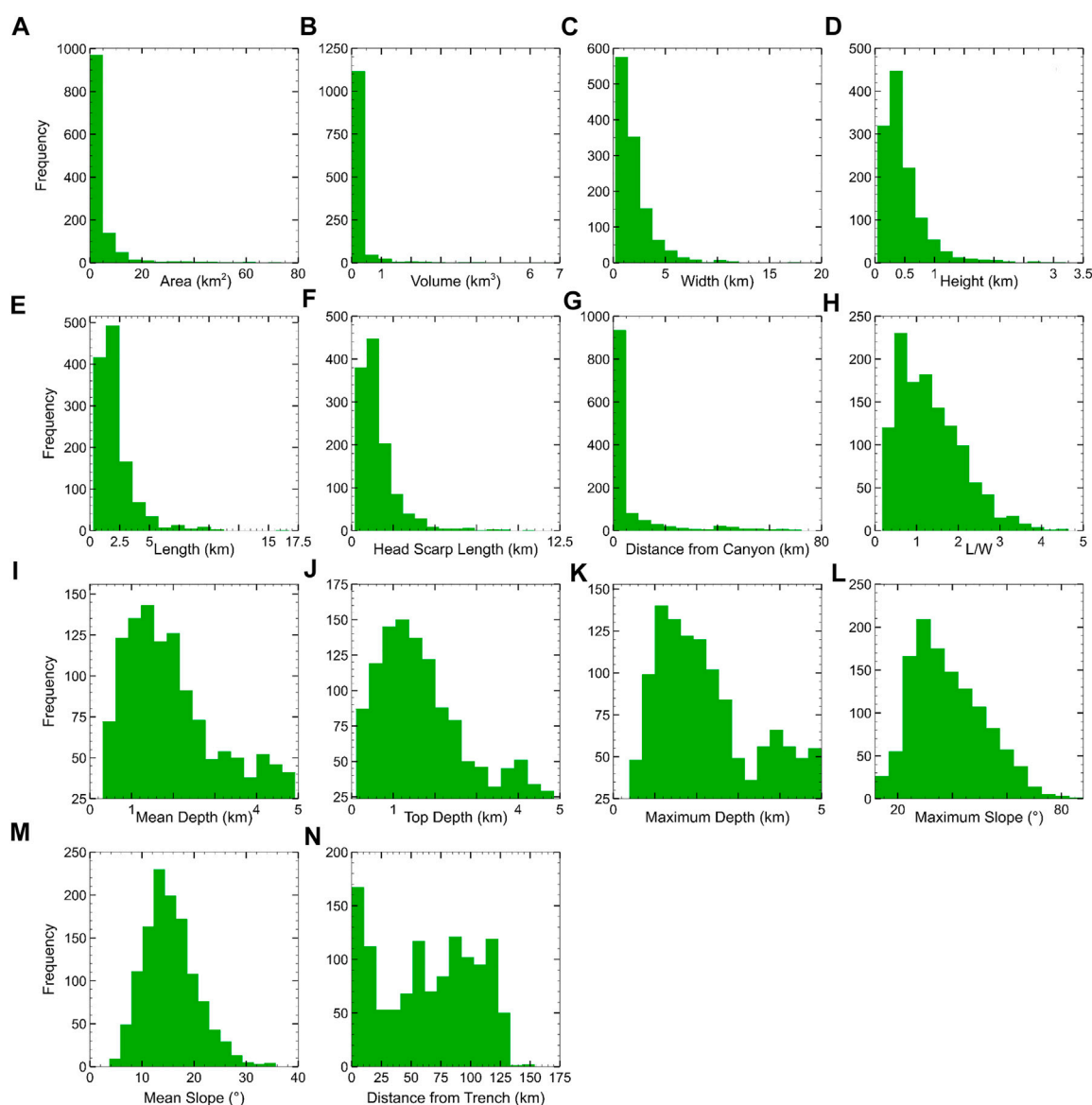


**FIGURE 7**

Histograms of submarine landslide morphometric parameters. (A) Area, (B) volume, (C) width, (D) height, (E) length, (F) head scarp length, and (G) distance from submarine canyons follow a power-law distribution, reflecting the ubiquitous small submarine landslides. (H) L/W ratio, (I–K) depth, and (L, M) slope show a positively skewed binomial distribution. On the other hand, the (N) distance from the trench has an irregular distribution.

reverse faults. Profile A–A' shows the collision and subsequent subduction of the Cagayan Ridge beneath the northern Negros Trench forearc. In profiles B–B' and C–C', the décollement and subduction of the southeast Sulu Sea along the frontal wedge are shown. Notably, profile C–C' also depicts a crustal splinter that is associated with intense thrusting and folding along this segment.

Four segments were delineated based on frontal wedge variations: (1) The northern Negros Trench (NT1) is northeast trending (15° azimuth) and transects between 10.86°N and 9.76°N with a length of about 126 km. This segment is bounded by the Cagayan Ridge seamount chain and southern Panay Island. Its frontal wedge has a maximum width of about 30 km and steepens subvertically northward. (2) The southern Negros Trench (NT2) is northwest trending (azimuth 340°), with a

length of 131 km and a maximum width of 15 km. (3) The northern Sulu Trench (ST1) is northeast trending (azimuth 19°) with a length of 146 km and a frontal wedge width of 20 km. (4) Lastly, the southern Sulu Trench (ST2) segment is east-northeast trending (azimuth 61°) with a length of about 170 km. Unlike the other segments, ST2 has a poorly developed frontal wedge with subparallel lineaments.

## 4.2 Morphometry of submarine landslides

Morphometric parameters that are size-dependent, i.e., area, volume, width, height, length, and head scarp length, all follow a power-law distribution with ubiquitous low values (Figures 7A–F).

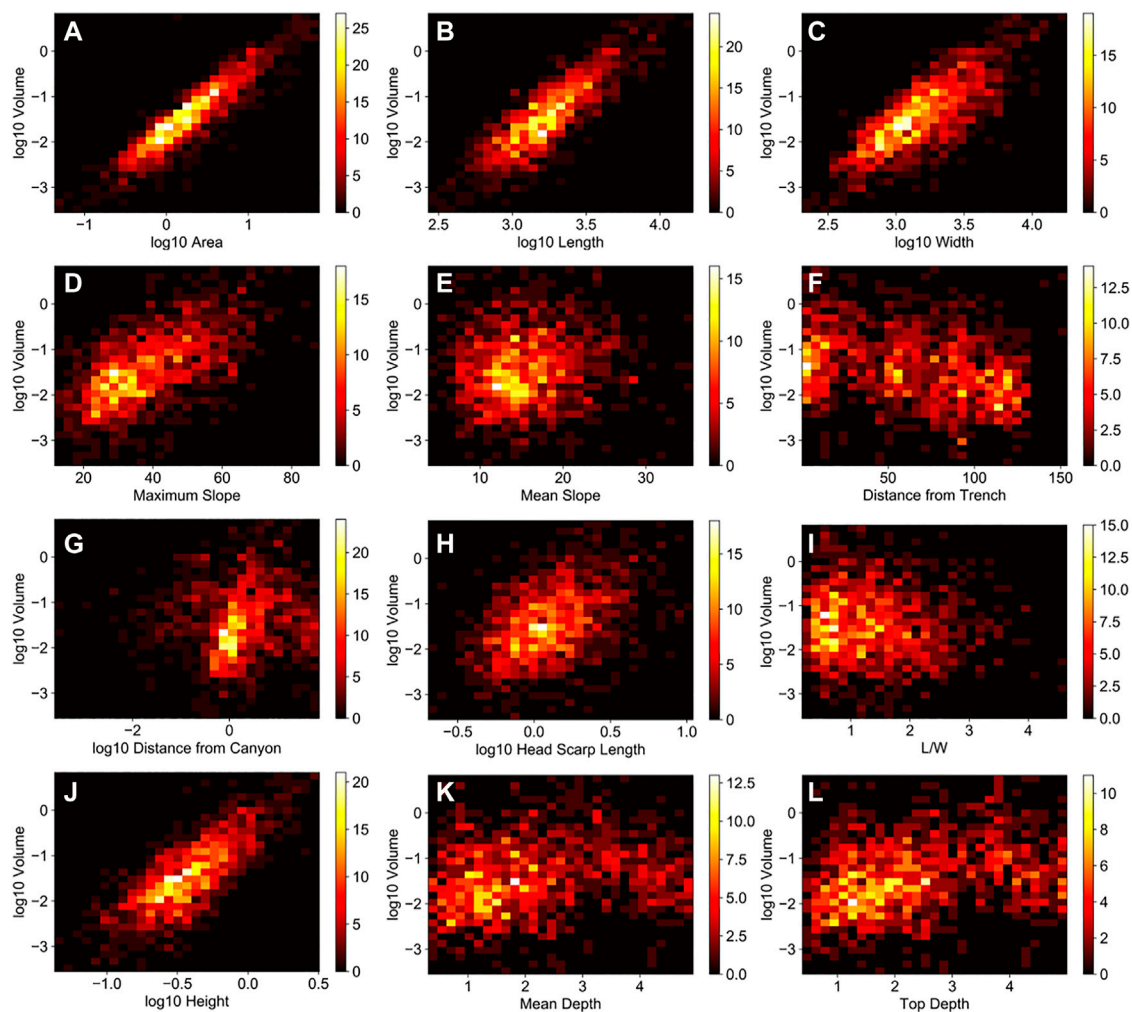


**FIGURE 8**

2D histograms of submarine landslide parameters with respect to volume (refer to Figure 7 for units). Size-dependent parameters such as (A) area, (B) length, (C) width, (H) head scarp length, and (J) height show a positive correlation with volume. The (D) maximum slope also shows a positive trend with volume. Other parameters (E-L) have a weak association with volume, but an apparent inverse trend can be observed with (F) distance from the trench and (I) L/W. Volume is observed to increase with (K, L) depth up to around 3 km and then shifts to a negative trend toward 5 km depth.

The distance from the submarine canyon also follows the same distribution. On the other hand, L/W, maximum slope, and mean, top, and maximum depth have skewed binomial distributions that peak around 1.4–1.8 km. Of the 1,214 submarine landslides, 78% have an area and volume of <math> < 5 \text{ km}^2 </math> and <math> < 0.5 \text{ km}^3 </math>, respectively (Figure 7). The mean area and volume are <math> 1.8 \text{ km}^2 </math> (median = <math> 4.0 \text{ km}^2 </math>) and <math> 0.03 \text{ km}^3 </math> (median = <math> 0.18 \text{ km}^3 </math>), respectively. The average maximum slope is <math> 38^\circ </math>, and the majority (23%) of distances from the trenches were <math> < 20 \text{ km} </math>. On the other hand, 77% of submarine landslides are less than 5 km away from submarine canyons.

Area, volume, length, width, distance from submarine canyons, head scarp length, and height were scaled logarithmically in the 2D histogram to normalize highly skewed power-law distributions. A base of 10 was arbitrarily chosen for the logarithmic normalization. Figure 8 and Figure 9 show the 2D histogram correlation relative to the volume and L/W, respectively, among morphometric parameters. Area, length, width, headscarp length, and height show positive correlations with volume as these are typically size-dependent. The

maximum slope is also positively correlated with volume. Although the plots were highly scattered, an apparent inverse trend is observed between volume and the distance from the trench and L/W. Top and mean depths show an apparent positive trend where volume increases with depth up to around 3 km and then shifts to an inverse pattern toward 5 km depth. For L/W correlations, the rest of the parameters have highly scattered plots, except for the apparent negative trend with respect to area, width, maximum slope, and distance from submarine canyons. In addition, an apparent positive trend is observed between length and L/W.

### 4.3 Spatial distribution and correlation of submarine features

Ripley's L function (Figure 10) shows higher observed  $L(\hat{L}_{\text{obs}(r)})$  than the expected ( $\hat{L}_{\text{theo}(r)}$ ) values, indicating a non-random distribution and clustering at a wide range of distances. This is

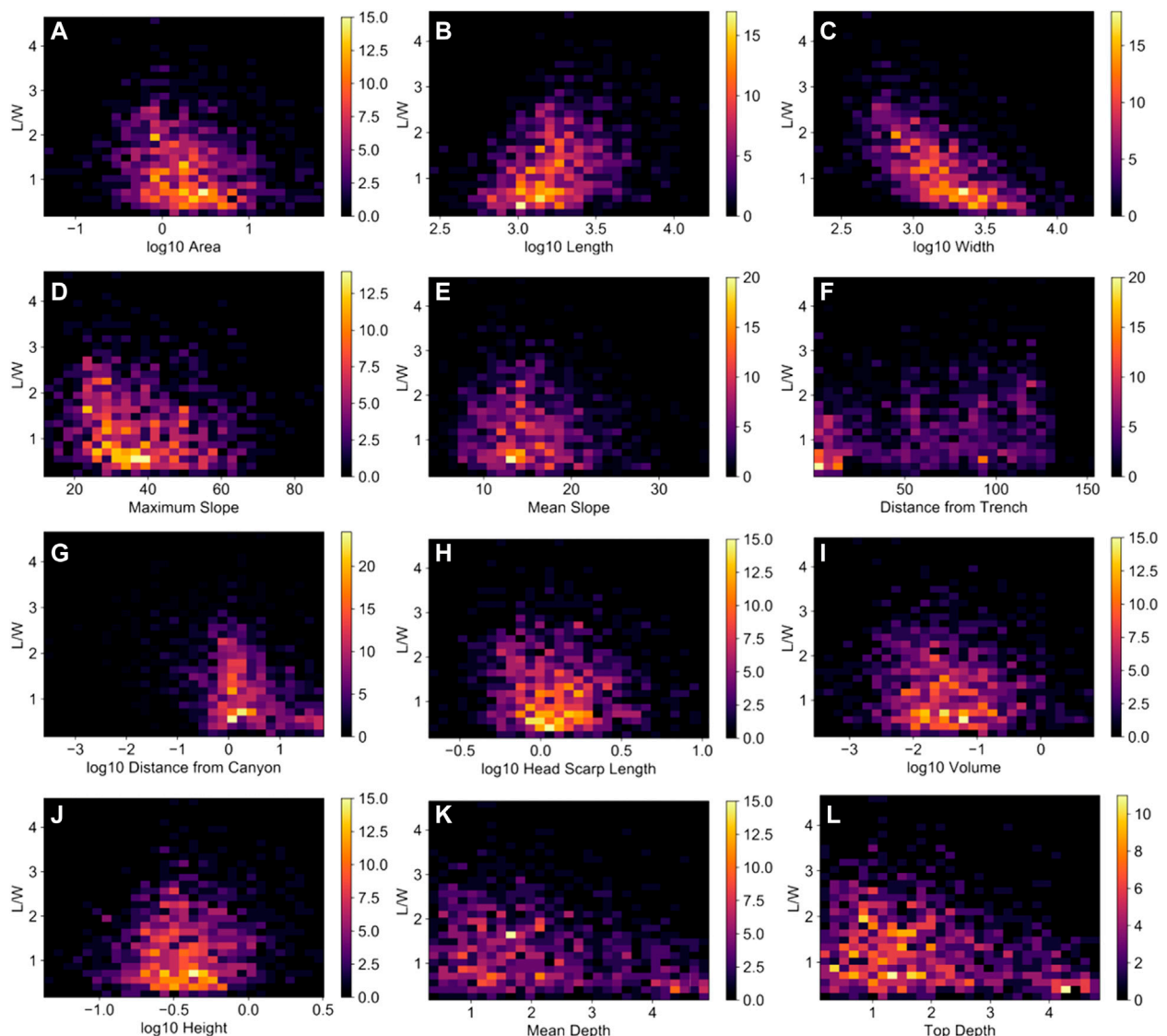


**FIGURE 9**

2D histograms of submarine landslide parameters with respect to the L/W (refer to Figure 7 for units). Majority of the parameters have highly scattered plots (E, F, H, I, J, K, L), although (A) area, (C) width, (D) maximum slope, and (G) distance from the submarine canyon show an apparent inverse trend. In addition, an apparent positive trend is observed in (B) length and L/W.

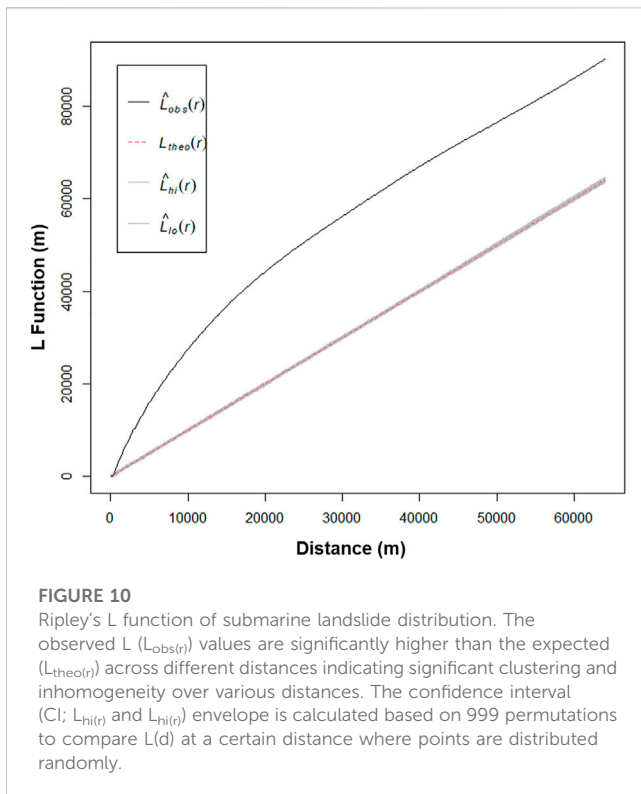
exemplified by the inhomogeneous kernel density of submarine landslides in Figure 11A. The highest intensity distribution of submarine landslides is located offshore between southeastern Negros Island and northern Zamboanga Peninsula, as well as between southern Panay and southwestern Negros islands. Submarine canyons also have a similar distribution to submarine landslides (Figure 11C), whereas lineaments (Figure 11B) are concentrated in the frontal wedge of the trench. Matrix correlation among kernel densities including earthquakes reveals that submarine canyons have the highest correlation (0.76) with the distribution of submarine landslides.

Regions with significant clusters of high and low volume and L/W based on Getis-Ord statistics are shown in Figure 12. Significantly large-volume ( $>0.5 \text{ km}^3$ ) submarine landslides are clustered offshore of southern Panay Island as well as offshore

southeastern Negros, Zamboanga Peninsula, and Sulu islands. On the other hand, those with a significantly small volume ( $<0.05 \text{ km}^3$ ) are concentrated where the highest probability density of submarine landslides and canyons occurs (Figures 11A,C, respectively). Significantly high L/W submarine landslides (Figure 12B) are clustered along areas with high kernel density of submarine canyons (Figure 11C). Those with significantly low L/W are clustered along the frontal wedge and abyssal plains.

#### 4.4 Significant clusters of high and low volume and L/W

Significant clusters of submarine landslides were grouped based on the degree of statistical significance (% CI), while their depth and



slope parameters were plotted in boxplots (Figure 13). Significant clusters of large-volume submarine landslides (90%, 95%, and 99% CI) have a wide interquartile range (IQR) of top and mean depths (Figures 13A, B), whereas significantly small-volume (90% and 95% CI) submarine landslides have a narrow IQR around 1–2 km depths. An opposite trend is observed for those with significantly high and low L/W ratios (Figures 13E, F). Submarine landslides with high L/W ratios (90%, 95%, 99% CI) have high distribution occurring at shallower depths, whereas those with low L/W ratios (90%, 95%, 99% CI) occur at deeper levels with a wider IQR. In terms of slope, those with significantly high volume have generally steeper mean and maximum slope than those with significantly low volume (Figures 13C, D). On the other hand, groups in terms of L/W have a similar range of mean slope (Figure 13G), but the maximum slope decreases with higher L/W ratios (Figure 13H).

## 5 Discussion

### 5.1 Frontal wedge variations along the NSTS

The well-developed frontal wedge of the three segments (NT1, NT2, ST1) of the NSTS is linked to relatively high sedimentation rates of this active margin demonstrated by dense networks of submarine canyons (i.e., conduits of inland clastic deposits) and low overall convergence rates (54 mm yr<sup>-1</sup>, NT; 28 mm yr<sup>-1</sup>, ST) based on previous GPS surveys (Rangin et al., 1999; Simons et al., 1999). High sediment influx and slow convergence rates (<60 mm yr<sup>-1</sup>) are conducive conditions in developing accretionary margins and frontal wedge (e.g., Huene and Scholl, 1991; Lallemand et al., 1994; Clift and Vannucchi 2004; Simpson

2010). In addition, morphological variations of the frontal wedge along the NSTS are attributed to the heterogeneity of sediment distribution from nearby islands and variability of convergence rates and forearc deformation. NT1, NT2, and ST1 segments are relatively closer to Panay, Guimaras, Negros, and Zamboanga Peninsula. These segments are presumed to receive higher sediment influx due to larger land areas than the ST2 segment which is closer to the smaller Sulu Group of Islands (Figure 1). Similar findings along the northern segments of both the Manila (Armada et al., 2020) and Japan (Tsuru et al., 2002; Kodaira et al., 2017) trenches also attributed the well-developed accretionary prism to higher sedimentation influx than the southern segments.

Another variation observed on the trench segments is their steepness, most notably on NT1, which is marked by an oversteepened frontal wedge. While well-developed frontal wedges have been correlated to high sediment influx and slow convergence rates, oversteepening is mainly driven by seamount subduction. These bathymetric highs cause intense uplift, deformation, and thrust faulting of the overriding plate inducing steepening and erosion (Yang et al., 2022). Examples of these frontal wedge oversteepening include segments of the Hikurangi Trough (Pedley et al., 2010), Java Trench (Masson et al., 1990), Middle America Trench (Hühnerbach et al., 2005), and Nankai Trough (Bangs et al., 2006; Moore et al., 2019). Similarly, the collision and subsequent subduction of the northeastern portion of the Cagayan Ridge along NT1 presumably induce oversteepening of the frontal wedge as well as its orientation change to the northeast.

The characteristics of the four trench segments based on frontal wedge variations provide essential information not only on the potential impacts of submarine landslides but also for modeling future megathrust tsunami scenarios. Furthermore, the width of the frontal wedge is indicative of its tsunami hazard potential as tsunami run-ups of shallow megathrust ruptures have been correlated to the width of the frontal wedge (Qiu and Barbot 2022). This is further emphasized by historical records where great offshore earthquakes occur mostly along accretionary prisms with thick sediment cover (Bilek and Lay 2018).

### 5.2 Controls of submarine landslide distribution

Exploratory spatial analyses revealed non-random and significant clustering of submarine landslides in which ubiquitous and small-volume landslides are controlled predominantly by submarine canyon systems. These conduits of terrestrial sedimentation influx induce overloading and instability to prolate slope failures. In addition, significant clustering of prolate (high L/W) submarine landslides coincides with the distribution of submarine canyon systems. The resemblance of prolate morphology to submarine canyons implies that these prolate submarine landslides influence the development of submarine canyon networks. Small submarine landslides may eventually interconnect forming incisions for sediment transportation (Baztan et al., 2005; Micallef et al., 2012). This relationship between prolate submarine landslides and submarine canyons is further supported by the apparent inverse trend between L/W and the distance from submarine canyons (Figure 9F). These

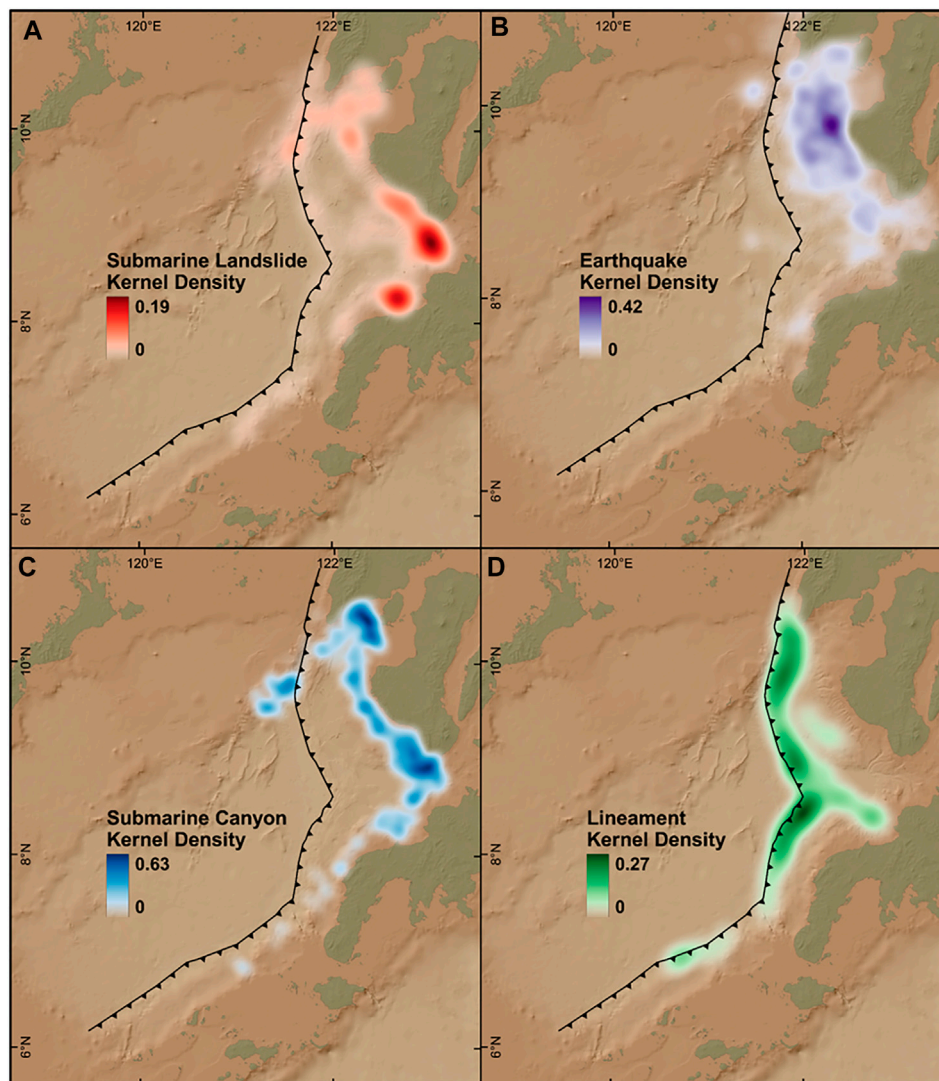


**FIGURE 11**

Kernel density variations (per km<sup>2</sup>) of (A) submarine landslides, (B) earthquakes, (C) submarine canyons, and (D) lineaments across the NSTS.

Earthquake kernel density is distributed mainly along the Negros Trench segments, whereas that of lineaments along the frontal wedge. Matrix band correlations showed that submarine canyons have the highest correlation to submarine landslide distribution of 0.76, followed by earthquakes (0.46) and then lineaments (0.20).

clustered submarine landslides with high L/W are prevalent in relatively shallower depths around 1–3 km where submarine canyons typically form. On the other hand, significant clusters of oblate (low L/W) submarine landslides mainly occur along the frontal wedge and in abyssal plains (Figure 12B). This is due to the subparallel and steep ridges along the frontal wedge that are suitable morphotectonic structures to form oblate submarine landslides.

While small landslides are mainly controlled by submarine canyons, large ones are significantly clustered along steep slopes and at varying depths. Most notably, the NT1 frontal wedge is marked by the densest cluster of large submarine landslides. As discussed in Section 5.1, this segment has an oversteepened and wide frontal wedge linked to the collision and subsequent subduction of Cagayan Ridge seamounts. Thus, we associate the seamount

subduction and subsequent slope oversteepening as dominant preconditioning factors for the occurrence of large submarine landslides along this segment. Modeling of seamount subduction beneath the accretionary prism, in its initial stage, resulted to oversteepening of the frontal wedge, reactivation of frontal thrust faults, and large submarine landslides (Dominguez et al., 2000; Ruh 2016; Morgan and Bangs 2017). This is supported by other accretionary prisms where seamount subduction underlies large submarine landslides (e.g., Hühnerbach et al., 2005; Pedley et al., 2010). While it is unclear what causes the clustering of large submarine landslides in other portions, the role of nearby fault structures (e.g., SCDL), intense tectonic deformation and fully subducted seamounts, together with sediment overloading could all play complex roles to induce steepening. Nonetheless, the identified regions with clusters of large submarine landslides

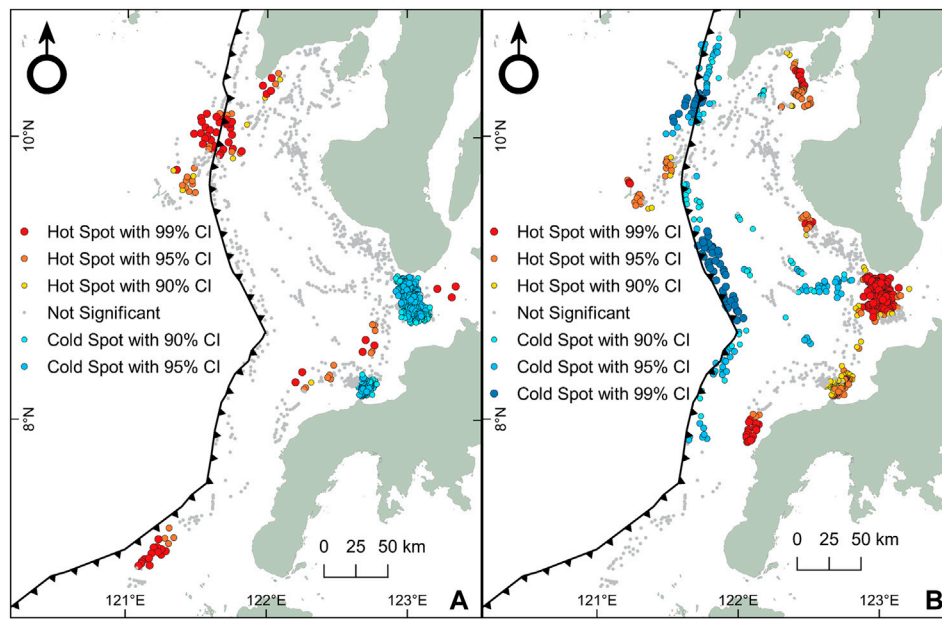


**FIGURE 12**

Getis-Ord ( $G_i^*$ ) analysis of submarine landslide distribution with respect to volume and L/W. **(A)** Significant clusters of large-volume submarine landslides (red dots) are found in different regions of the active margin, but the densest clusters are in the northern NT segment (NT1), where collision with the Cagayan Ridge occurs. Significant clusters of small-volume submarine landslides (blue dots) are located offshore of Negros Island and Zamboanga Peninsula, corresponding to areas with the densest submarine canyon systems (Figure 11A). **(B)** Significant clusters of high L/W (red dots) are also in regions with dense submarine canyon systems. On the other hand, the frontal wedge and abyssal plain host significant clusters of low L/W (blue dots).

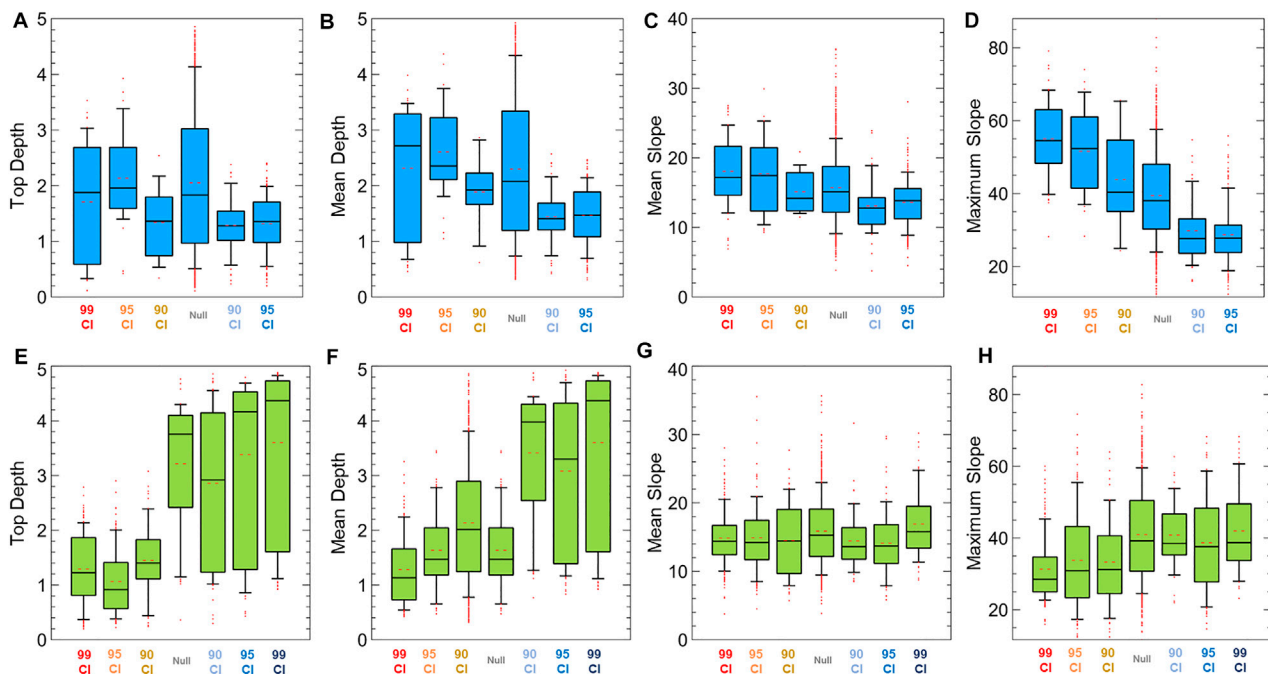


**FIGURE 13**

Boxplots showing the depth and slope of submarine landslides that are grouped based on the  $G_i^*$  statistic (blue boxplots, based on volume; yellow green, based on L/W) in Figure 13 (red hue, hot spots; blue hue, cold spots). Red dots indicate the outliers, while broken lines inside the interquartile range (IQR) show the mean value. **(A–D)** Box plots based on the volume show that significant clusters of large submarine landslides have depths with wide IQR (0.1–4 km), while small ones are in a narrow IQR of about 0.1–2 km. Mean slope **(C)** tends to concentrate between  $10^\circ$  and  $30^\circ$  with slightly lower values for significantly small-volume submarine landslides. **(D)** Maximum slope showed a positive association with clusters of significantly large-volume submarine landslides, whereas small-volume landslides have a lower maximum slope. **(E–H)** Clusters of significantly high L/W occur in shallower depths and slightly lower slopes than those of significantly low L/W.

provide significant insights into modeling landslide-driven tsunamis, where the estimated volume is highly correlated with potential tsunami wave height (Sabeti and Heidarzadeh 2022).

This study highlights the dominant role of submarine canyon systems due to high sediment influx and subduction-induced oversteepening to precondition slope instability. As the slope becomes unstable, gravity and earthquakes can readily trigger submarine failures along active margins (Masson et al., 2006; Scarselli 2020). The possible presence of gas hydrates may also be involved as they occur along margins with high sedimentation influx (e.g., Gee et al., 2007; Mountjoy et al., 2014; Crutchley et al., 2016). Thus, we recommend dense seismic reflection surveys to further map the underlying structures and their variations across the active margin in detail. In addition, the current resolution of bathymetry data is inadequate to map even smaller (m-scale) submarine landslides. This has been shown by the absence of significant clusters of small submarine landslides at 99% CI. As bathymetry resolution has been a common limitation in mapping submarine landslides (e.g., Gazioglu et al., 2005; Watson et al., 2020; Gamboa et al., 2022), higher-resolution multibeam bathymetry surveys will further improve the characterization of submarine geomorphological features.

## 6 Conclusion

Four frontal wedge segments were delineated in the NSTS, with varying widths, lengths, and associated morphotectonic features. These variations are linked to the disparity of convergence rates along the trench, subduction processes, and heterogeneous distribution of sediments from inland sources. A total of 1,214 submarine landslides and their morphometric parameters along this active margin were delineated. Prolate submarine landslides (high L/W) tend to form in submarine canyons, whereas oblate morphologies (low L/W) generally occur along the frontal wedge and abyssal plains. These opposing submarine landslide morphologies reflect their different environments and geomorphological conditions.

Ubiquitous small submarine landslides are mainly controlled by submarine canyon systems where high sediment influx from inland sources preconditions instability. These small-volume submarine landslides also occur in relatively shallow depths of about 1–2 km and generally have a lower mean and maximum slope. On the other hand, seamount subduction and related tectonic processes that induce oversteepening play dominant role to precondition large submarine landslides. This study revealed the influence of spatial, geomorphological, and tectonic controls to the morphological variations of submarine landslides in the active margin. Furthermore, the identified regions with clustered large submarine landslides and the segments of the NSTS provide essential information in modeling fault and submarine failure-driven tsunamis and identification of highly exposed coastal areas. This study also demonstrates the use of morphological and exploratory spatial analyses to elucidate underlying controlling factors and to evaluate the hazard potential of areas with limited geological and geophysical datasets.

## Data availability statement

The original contributions presented in the study are included in the article/supplementary material, further inquiries can be directed to the corresponding author.

## Author contributions

LN and NR contributed to the conceptualization and structure of the study. LN wrote the first draft of the manuscript and performed the terrain and statistical analyses. Both authors contributed to the manuscript writing and revision and have read and approved the submitted version.

## Funding

This study is supported by the 2022 NIGS Research Grant “Investigating the frontal wedge characteristics and geological controls of submarine landslides in the Negros–Sulu Trench System”, funded by the University of the Philippines Diliman and “Investigation and Numerical Modeling of Philippine Tsunamis Based on Historical, Geomorphological, and Geological Evidence of Past Earthquakes Investigation and Numerical Modeling of Philippine Tsunamis” (No. 4233), funded by the Department of Science and Technology (DOST) through the DOST–Philippine Council for Industry, Energy, and Emerging Technology Research and Development (DOST-PCIEERD).

## Acknowledgments

The authors would like to acknowledge the Philippine National Mapping and Resource Information Authority (NAMRIA) for providing multibeam bathymetry data, as well as the PHIVOLCS for the seismicity and onshore fault data. We are grateful to Editor RA and reviewers DD and WL for their insightful comments that have greatly improved the content and structure of the manuscript. We also thank D. Gamboa for providing valuable insights in the parameterization of submarine landslides in this study. The ArcGIS Pro software was utilized through the academic license acquired by the University of the Philippines Diliman. We would also like to acknowledge the following open-source libraries, software, and processing tools that were used in this study: Veusz, Jupyter, spatstat (R), and Python libraries: Matplotlib, NumPy, Pandas, and math; QGIS plug-ins: Profile Tool, Qgis2threejs, and Volume Calculation Tool.

## Conflict of interest

The authors declare that the research was conducted in the absence of any commercial or financial relationships that could be construed as a potential conflict of interest.

## Publisher's note

All claims expressed in this article are solely those of the authors and do not necessarily represent those of their affiliated

organizations, or those of the publisher, the editors and the reviewers. Any product that may be evaluated in this article, or claim that may be made by its manufacturer, is not guaranteed or endorsed by the publisher.

## References

- Armada, L. T., Hsu, S. K., Dimalanta, C. B., Yumul, G. P., Doo, W. B., Yeh, Y. C., et al. (2020). Forearc structures and deformation along the Manila trench. *J. Asian Earth Sci.* *X* 4, 100036. doi:10.1016/j.jaesx.2020.100036
- Baba, T., Gon, Y., Imai, K., Yamashita, K., Matsuno, T., Hayashi, M., et al. (2019). Modeling of a dispersive tsunami caused by a submarine landslide based on detailed bathymetry of the continental slope in the Nankai Trough, southwest Japan. *Tectonophysics* *768*, 228182. doi:10.1016/j.tecto.2019.228182
- Bangs, N. L. B., Gulick, S. P. S., and Shipley, T. H. (2006). Seamount subduction erosion in the Nankai Trough and its potential impact on the seismogenic zone. *Geology* *34* (8), 701–704. doi:10.1130/G22451.1
- Bautista, M. L. P., Bautista, B. C., Joan, S., and Narag, I. (2012). *Philippine tsunamis and seiches (1589-2012)*.
- Baztan, J., Berné, S., Olivet, J. L., Rabineau, M., Aslanian, D., Gaudin, M., et al. (2005). Axial incision: The key to understand submarine canyon evolution (in the western gulf of lion). *Mar. Petroleum Geol.* *22* (6–7), 805–826. doi:10.1016/j.marpetgeo.2005.03.011
- Bellon, H., and Rangin, C. (1991). Geochemistry and isotopic dating of cenozoic volcanic arc sequences around the Celebes and Sulu seas. *Proc., Sci. Results, ODP, Leg 124, Celebes Sulu Seas* *124*, 321–338. doi:10.2973/odp.proc.sr.124.163.1991
- Bilek, S. L., and Lay, T. (2018). Subduction zone megathrust earthquakes. *Geosphere* *14* (4), 1468–1500. doi:10.1130/GES01608.1
- Clift, P., and Vannucchi, P. (2004). Controls on tectonic accretion versus erosion in subduction zones: Implications for the origin and recycling of the continental crust. *Rev. Geophys.* *42* (2). doi:10.1029/2003RG000127
- Crutchley, G. J., Mountjoy, J. J., Gorman, A. R., Pecher, I. A., and Henrys, Stuart A. (2016). Submarine slope instabilities coincident with shallow gas hydrate systems: Insights from New Zealand examples. *Submar. Mass Movements Their Consequences. Adv. Nat. Technol. Hazards Res.* Vol. 41. Cham: Springer, 401–409. doi:10.1007/978-3-319-20979-1\_40
- Dominguez, S., Malavieille, J., and Lallemand, S. E. (2000). Deformation of accretionary wedges in response to seamount subduction: Insights from sandbox experiments. *Tectonics* *19* (1), 182–196. doi:10.1029/1999TC900055
- Fryer, G. J., Watts, P., and Pratson, L. F. (2004). Source of the great tsunami of 1 april 1946: A landslide in the upper aleutian forearc. *Mar. Geol.* *203* (3–4), 201–218. doi:10.1016/S0025-3227(03)00305-0
- Gamboa, D., Omira, R., and Pedro, T. (2022). Spatial and morphometric relationships of submarine landslides offshore west and southwest iberia. *Landslides* *19* (2), 387–405. doi:10.1007/s10346-021-01786-3
- Gazioglu, C., Yücel, Z. Y., and Doğan, E. (2005). Morphological features of major submarine landslides of marmara Sea using multibeam data. *J. Coast. Res.* *21* (4), 664–673. doi:10.2112/03-0060.1
- Gee, M. J. R., Uy, H. S., Warren, J., Morley, C. K., and Lambiasi, J. J. (2007). The Brunei slide: A giant submarine landslide on the north west borneo margin revealed by 3D seismic data<sup>246</sup>: 9–23. doi:10.1016/j.margeo.2007.07.009
- Getis, A., and Ord, J. K. (1992). The analysis of spatial association by use of distance statistics. *Geogr. Anal.* *24* (3), 189–206. doi:10.1111/j.1538-4632.1992.tb00261.x
- Hall, R. (2002). Cenozoic geological and plate tectonic evolution of SE asia and the SW pacific: Computer-based reconstructions, model and animations. *J. Asian Earth Sci.* *20* (4), 353–431. doi:10.1016/S1367-9120(01)00069-4
- Hall, R. (2013). Contraction and extension in northern borneo driven by subduction rollback. *J. Asian Earth Sci.* *76*, 399–411. doi:10.1016/j.jseas.2013.04.010
- Hall, R. (2012). Late jurassic–cenozoic reconstructions of the Indonesian region and the Indian ocean. *Tectonophysics* *570–571*, 5701–57141. doi:10.1016/j.tecto.2012.04.021
- Harbitz, C. B., Finn, L., and Hilmar, B. (2014). Submarine landslide tsunamis: How extreme and how likely? *Nat. Hazards* *72* (3), 1341–1374. doi:10.1007/s11069-013-0681-3
- Heinrich, P. H., Piatanesi, A., and Hébert, H. (2001). Numerical modelling of tsunami generation and propagation from submarine slumps: The 1998 Papua New Guinea event. *Geophys. J. Int.* *145* (1), 97–111. doi:10.1111/j.1365-246X.2001.00336.x
- Hidayat, D., Barker, J. S., and Satake, K. (1995). Modeling the seismic source and tsunami generation of the december 12, 1992 Flores island, Indonesia, earthquake. *Pure Appl. Geophys. PAGEOPH* *144* (3–4), 537–554. doi:10.1007/BF00874382
- Horn, B. K. P. (1981). Hill shading and the reflectance map. *Proc. IEEE* *69* (1), 14–47. doi:10.1109/proc.1981.11918
- Huene, Roland von, and Scholl, David W. (1991). Observations at convergent margins concerning sediment subduction, subduction erosion, and the growth of continental crust. *Rev. Geophys.* *29* (3), 279. doi:10.1029/91RG00969
- Hühnerbach, V., Masson, D. G., Bohrmann, G., Bull, J. M., and Weinrebe, W. (2005). Deformation and submarine landsliding caused by seamount subduction beneath the Costa Rica continental margin - new insights from high-resolution sidescan sonar data. *Geol. Soc. Spec. Publ.* *244*, 195–205. doi:10.1144/GSL.SP.2005.244.01.12
- Imamura, F., Gica, E., Takahashi, T., and Shuto, N. (1995). Numerical simulation of the 1992 Flores tsunami: Interpretation of tsunami phenomena in northeastern Flores island and damage at babi island. *Pure Appl. Geophys. PAGEOPH* *144* (3–4), 555–568. doi:10.1007/BF00874383
- Kao, H., Huang, G. C., and Liu, C. S. (2000). Transition from oblique subduction to collision in the northern Luzon arc-taiwan region: Constraints from bathymetry and seismic observations. *J. Geophys. Res. Solid Earth* *105* (B2), 3059–3079. doi:10.1029/1999jb900357
- Kawamura, K., Sasaki, T., Kanamatsu, T., Sakaguchi, A., and Ogawa, Y. (2012). Large submarine landslides in the Japan Trench: A new scenario for additional Tsunami generation. *Geophys. Res. Lett.* *39* (5), 3–7. doi:10.1029/2011GL050661
- Kodaira, S., Nakamura, Y., Yamamoto, Y., Obana, K., Gou, F., No, T., et al. (2017). Depth-varying structural characters in the rupture zone of the 2011 tohoku-oki earthquake. *Geosphere* *13* (5), 1408–1424. doi:10.1130/GES01489.1
- Kopp, H., Flueh, E. R., Petersen, C. J., Weinrebe, W., Wittwer, A., and Meramex Scientists (2006). The Java margin revisited: Evidence for subduction erosion off Java. *Earth Planet. Sci. Lett.* *242* (1–2), 130–142. doi:10.1016/j.epsl.2005.11.036
- Lai, C. K., XiaoXia, P., Hall, R., Meffre, S., Tsikouras, B., Balangué-Tarriela, M. I. R., et al. (2021). Cenozoic evolution of the Sulu Sea arc-basin system: An overview. *Tectonics* *40* (2), 1–26. doi:10.1029/2020TC006630
- Lallemand, S. E., Schnürle, P., and Malavieille, J. (1994). Coulomb theory applied to accretionary and nonaccretionary wedges: Possible causes for tectonic erosion and/or frontal accretion. *J. Geophys. Res. Solid Earth* *99* (B6), 12033–12055. doi:10.1029/94JB00124
- Liu, W. N., Li, C. F., Li, J., Fairhead, D., and Zhou, Z. (2014). Deep structures of the palawan and Sulu Sea and their implications for opening of the South China sea. *Mar. Petroleum Geol.* *58* (PB), 721–735. doi:10.1016/j.marpetgeo.2014.06.005
- Løvholt, F., Stein, B., Laberg, J. S., Kim, J., and Noel, B. (2017). Some giant submarine landslides do not produce large tsunamis. *Geophys. Res. Lett.* *44* (16), 8463–8472. doi:10.1002/2017GL074062
- Masson, D. G., Harbitz, C. B., Wynn, R. B., Pedersen, G., and Løvholt, F. (2006). Submarine landslides: Processes, triggers and hazard prediction. *Philosophical Trans. R. Soc. A Math. Phys. Eng. Sci.* *364* (1845), 2009–2039. –39. doi:10.1098/rsta.2006.1810
- Masson, D. G., Parson, L. M., Milsom, J., Nichols, G., Sikumbang, N., Dwiyanto, B., et al. (1990). Subduction of seamounts at the Java Trench: A view with long-range sidescan sonar. *Tectonophysics* *185* (1–2), 51–65. doi:10.1016/0040-1951(90)90404-V
- Micallef, Aaron, J Mountjoy, Joshu, Canals, Miquel, and Lastras, Galderic (2012). “Deep-seated bedrock landslides and submarine canyon evolution in an active tectonic margin: Cook strait, New Zealand,” in *Submarine mass movements and their consequences. Yujiro ogawa, roger urgeles, david mosher, jason chaytor, and michael strasser, 201–12*. Editors Yasuhiro Yamada, Kiichiro Kawamura, and Ken Ikehara (Dordrecht: Springer Netherlands). doi:10.1007/978-94-007-2162-3\_18
- Moore, G. F., JasonLackey, K., Strasser, M., and Yamashita, M. 2019. “Submarine landslides on the Nankai Trough accretionary prism (offshore central Japan).” 247–259. doi:10.1002/9781119500513.ch15
- Morgan, J. K., and Bangs, N. L. (2017). Recognizing seamount-forearc collisions at accretionary margins: Insights from discrete numerical simulations. *Geology* *45* (7), 635–638. doi:10.1130/G38923.1
- Mountjoy, J. J., Barnes, P. M., and Pettinga, J. R. (2009). Morphostructure and evolution of submarine canyons across an active margin: Cook strait sector of the Hikurangi margin, New Zealand. *Mar. Geol.* *260* (1–4), 45–68. doi:10.1016/j.margeo.2009.01.006
- Mountjoy, J. J., Pecher, I., Henrys, S., Crutchley, G., Barnes, P. M., and Plaza-Faverola, A. (2014). Shallow methane hydrate system controls ongoing, downslope sediment transport in a low-velocity active submarine landslide complex, Hikurangi margin, New Zealand. *Geochem. Geophys. Geosystems* *15* (11), 4137–4156. doi:10.1002/2014GC005379

- Nakata, K., Katsumata, A., and Muhari, A. (2020). Submarine landslide source models consistent with multiple tsunami records of the 2018 palu tsunami, Sulawesi, Indonesia. *Earth, Planets Space* 72 (1), 44. doi:10.1186/s40623-020-01169-3
- Parsons, T., Geist, E. L., Ryan, H. F., Lee, H. J., Haeussler, P. J., Lynett, P., et al. (2014). Source and progression of a submarine landslide and tsunami: The 1964 great Alaska earthquake at Valdez. *J. Geophys. Res. Solid Earth* 119 (11), 8502–8516. doi:10.1002/2014JB011514
- Pedley, K. L., Barnes, P. M., Pettinga, J. R., Lewis, K. B., and Lewis, K. B. (2010). Seafloor structural geomorphic evolution of the accretionary frontal wedge in response to seamount subduction, poverty indentation, New Zealand. *Mar. Geol.* 270 (1–4), 119–138. doi:10.1016/j.margeo.2009.11.006
- Pubellier, M., Quebral, R., Aurelio, M., and Rangin, C. (1996). Docking and post-docking escape tectonics in the southern Philippines. *Geol. Soc. Spec. Publ.* 106 (106), 511–523. doi:10.1144/GSL.SP.1996.106.01.32
- Qiu, Q., and Barbot, S. (2022). Tsunami excitation in the outer wedge of global subduction zones. *Earth-Science Rev.* 230, 104054. doi:10.1016/j.earscirev.2022.104054
- Ramirez, A. B. G., Ramos, N. T., Nawanao, L. P. J., Mangahas-Flores, R. Z., Narag, I. C., Baba, T., et al. (2022). An earthquake-triggered submarine mass failure mechanism for the 1994 Mindoro tsunami in the Philippines: Constraints from numerical modeling and submarine geomorphology. *Front. Earth Sci.* 10, 1–20. doi:10.3389/feart.2022.1067002
- Rangin, C., and Silver, E. (1990). Geological setting of the Celebes and Sulu seas. *Proc. Ocean Drill. Program Initial Rep.*, 124. Ocean Drilling Program. doi:10.2973/odp.proc.ir.124.103.1990
- Rangin, C., and Silver, E. A. (1991). Neogene tectonic evolution of the Celebes-Sulu basins: New insights from leg 124 drilling. *Proc. Ocean Drill. Program Scientific Results*. 124. Ocean Drilling Program, 51–63. doi:10.2973/odp.proc.sr.124.122.1991
- Rangin, C. (1989). The Sulu Sea, a back-arc basin setting within a neogene collision zone. *Tectonophysics* 161 (1–2), 119–141. doi:10.1016/0040-1951(89)90307-7
- Rangin, C. X., Mazzotti, S., Pubellier, M., Aurelio, M., Walpersdorf, A., and Quebral, R. (1999). Plate convergence measured by GPS across the Sundaland/Philippine Sea plate deformed boundary: The Philippines and eastern Indonesia, 296–316.
- Rastgoftar, E., and Soltanpour, M. (2016). Study and numerical modeling of 1945 Makran tsunami due to a probable submarine landslide. *Nat. Hazards* 83 (2), 929–945. doi:10.1007/s11069-016-2356-3
- Ripley, B. D. (1977). Modelling spatial patterns. *J. R. Stat. Soc.* 39=39 (2), 172–192. Available at: <https://www.jstor.org/stable/2984796>. doi:10.1111/j.2517-6161.1977.tb01615.x
- Ruh, J. B. (2016). Submarine landslides caused by seamounts entering accretionary wedge systems. *Terra Nova* 28 (3), 163–170. doi:10.1111/ter.12204
- Sabeti, R., and Heidarzadeh, M. (2022). A new empirical equation for predicting the maximum initial amplitude of submarine landslide-generated waves. *Landslides* 19 (2), 491–503. doi:10.1007/s10346-021-01747-w
- Scarselli, N. (2020). Submarine landslides – architecture, controlling factors and environments. A summary. *Regional geology and tectonics: Principles of geologic analysis*. BV. doi:10.1016/b978-0-444-64134-2.00015-8
- Schambach, L., Grilli, S. T., Tappin, D. R., Gangemi, M. D., and Barbaro, G. (2020). New simulations and understanding of the 1908 Messina tsunami for a dual seismic and deep submarine mass failure source. *Mar. Geol.* 421, 106093. doi:10.1016/j.margeo.2019.106093
- Schlüter, H. U., Block, M., Hinz, K., Neben, S., Seidel, D., and Djajadihardja, Y. (2001). Neogene sediment thickness and Miocene basin-floor fan systems of the Celebes Sea. *Mar. Petroleum Geol.* 18 (7), 849–861. doi:10.1016/S0264-8172(01)00027-7
- Schlüter, H. U., Hinz, K., and Block, M. (1996). Tectono-stratigraphic terranes and detachment faulting of the South China Sea and Sulu Sea. *Mar. Geol.* 130 (1–2), 39–78. doi:10.1016/0025-3227(95)00137-9
- Silverman, B. W. (1986). *Density estimation for statistics and data analysis*. Boston, MA: Springer US. doi:10.1007/978-1-4899-3324-9
- Simons, W. J. F., Ambrosius, B. A. C., Noomen, R., Angermann, D., Wilson, P., Becker, M., et al. (1999). Observing Plate motions in S.E. Asia: Geodetic results of the GEODYSSSEA project. *Geophys. Res. Lett.* 26 (14), 2081–2084. doi:10.1029/1999GL00395
- Simpson, G. D. H. (2010). Formation of accretionary prisms influenced by sediment subduction and supplied by sediments from adjacent continents. *Geology* 38 (2), 131–134. doi:10.1130/G30461.1
- Takagi, H., Pratama, M. B., Kurobe, S., Esteban, M., Aránguiz, R., and Ke, B. (2019). Analysis of generation and arrival time of landslide tsunami to Palu city due to the 2018 Sulawesi earthquake. *Landslides*. March: 983–91. doi:10.1007/s10346-019-01166-y
- Tappin, D. R., Stephan, T. G., Harris, J. C., Geller, R. J., Masterlark, T., Kirby, J. T., et al. (2014). Did a submarine landslide contribute to the 2011 Tohoku tsunami? *Mar. Geol.* 357, 344–361. doi:10.1016/j.margeo.2014.09.043
- Tappin, D. R. (2021). Submarine landslides and their tsunami hazard. *Annu. Rev. Earth Planet. Sci.* 49 (1), 551–578. doi:10.1146/annurev-earth-063016-015810
- Tsuru, T., Park, J.-O., Miura, S., Kodaira, S., Kido, Y., and Hayashi, T. (2002). Along-Arc structural variation of the plate boundary at the Japan trench margin: Implication of interplate coupling. *J. Geophys. Res. Solid Earth* 107 (B12), ESE 11–1–ESE 11–15. doi:10.1029/2001jb001664
- Vanneste, M., Forsberg, C. F., Glimsdal, S., Harbitz, C. B., Issler, D., Kvalstad, T. J., et al. (2013). Submarine landslides and their consequences: What do we know, what can we do? *Landslide Sci. Pract. Complex Environ.* 5, 5–17. doi:10.1007/978-3-642-31427-8\_1
- Völker, D. J. (2010). A simple and efficient GIS tool for volume calculations of submarine landslides. *Geo-Mar. Lett.* 30 (5), 541–547. doi:10.1007/s00367-009-0176-0
- Watson, S. J., Mountjoy, J. J., and Crutchley, G. J. (2020). Tectonic and geomorphic controls on the distribution of submarine landslides across active and passive margins, eastern New Zealand. *Geol. Soc. Lond. Spec. Publ.* 500 (1), 477–494. doi:10.1144/SP500-2019-165
- Yang, G., Si, G., Tong, L., Li, H., Lindagato, P., and Zeng, R. (2022). The effect of seamount chain subduction and accretion. *Geol. J.* 57 (7), 2712–2734. doi:10.1002/gj.4435
- Yavari-Ramshe, S., and Ataie-Ashtiani, B. (2016). Numerical modeling of subaerial and submarine landslide-generated tsunami waves—recent advances and future challenges. *Landslides* 13 (6), 1325–1368. doi:10.1007/s10346-016-0734-2